Production of Janus/Hecate microfibers by microfluidic photopolymerization and evaluation of their potential in dyes removal

Wasif Razzaq, Christophe Serra, Delphine Chan-Seng

Production of Janus/Hecate microfibers by microfluidic photopolymerization and evaluation of their potential in dyes removal

Wasif Razzaq,[a,b] Christophe Serra,[a,*] Delphine Chan-Seng[a,*]

[a] *Université de Strasbourg, CNRS, Institut Charles Sadron UPR 22, F-67000 Strasbourg, France*
* ca.serra@unistra.fr; delphine.chan-seng@ics-cnrs.unistra.fr

[b] *Department of Materials, National Textile University, Sheikhupura Road, Faisalabad, 37610, Pakistan*

The microfluidic production of Janus/Hecate polymer microfibers with well-defined interfaces from miscible phases is reported. The process offers tunability of the width and composition of each part of the fibers by controlling in a single step the flow rate and nature of the monomers. The enhanced performances of the fibers are outlined for the simultaneous removal of dyes of opposite charges using amphoteric Janus fibers.

Microfibers have gained significant attention due to their potential in applications such as biomedicine[1] and sensors,[2, 3] mainly because of their high surface to volume ratio. The development of structurally anisotropic microfibers increasingly strives to achieve fibers of different chemical natures and physical properties to overcome the limited performances of fibers based on a single material.[4, 5] Among them, Janus fibers represent a great opportunity to access new properties and applications, but the routes to prepare them are still limited. Most reports focus on electrohydrodynamic processes including side-by-side electrospinning,[6-11] conjugate electrospinning,[12] microfluidic electrospinning,[13] and other conventional techniques such as direct jetting[14] and melt spinning.[15] Their main limitations are (i) the access to diameters in the submicrometer range only, (ii) the incompatibility with biological systems due to high voltage, temperature, and use of solvent, and (iii) the restriction to pre-existing polymers in the presence of a suitable solvent.

Microfluidic spinning is an emerging and promising technique for the continuous fabrication of microfibers. It proceeds by establishing the co-flow between a core phase (Φ_{core}) that will form the fiber material and a sheath phase (Φ_{sheath}) which hydrodynamically “spins” the fiber thanks to a microfluidic device. This technique offers advantages over conventional ones such as complete control on the diameter/volume ratio by tuning the flow rates of both core and sheath

fluids,[16] multiple solidification methods,[3] easy hydrogel formation,[17] micro- to submicron size range,[18] and compatibility with biological systems.[19] Fibers produced by microfluidic spinning relying on immiscible fluids provide access to jetting conditions only in a very narrow range of flow rates to obtain fibers and thus limits the use of multiple core phases due to the existence of very different interfacial tensions.[20-22] Reports using purely miscible core and sheath phases describe the preparation of only single and Janus fibers based on alginate,[23-26] and also hollow[27] and mosaicked[24] fibers from poly(ethylene glycol) diacrylate until now. However, the preparation of Janus fibers, fibers with a side-by-side arrangement joined at the interface with two parts of different composition offering the possibility to develop materials with unique properties (*e.g.* differentiated encapsulation abilities and compartmentalized properties), from monomers using miscible fluids has not yet been reported even though this strategy would significantly widen the type of Janus fibers (chemical nature of the different phases, one-step production of hydrogel, etc.) that could be obtained.

Herein we report the use of a side-by-side capillaries-based microfluidic device operating with different miscible phases (core monomer phases) co-flowing with the continuous (sheath) phase to produce Janus and Hecate microfibers. Two photopolymerizable monomer systems were used as core phase 1 (Φ_{core1}) and core phase 2 (Φ_{core2}). Φ_{core1} was composed of tri(propylene glycol) diacrylate (TPGDA, 80 %v), ethanol (20 %v), Irgacure 369 (3 %w/v) as photoinitiator, while Φ_{core2} was composed of NOA89 (photocurable acrylate-terminated prepolymer) (80 %v) and ethanol (20 %v). Poly(ethylene glycol) with a molecular weight of 300 g/mol (PEG300) was used as the sheath phase. The core phases were injected at specific flow rates through capillary 1 and capillary 2 arranged side-by-side using syringes pumps (Fig. 1). Φ_{core1} and Φ_{core2} exited at the tip of their respective capillary and got in contact to each other spontaneously forming two parallel streams of monomers due to shear imposed by the sheath fluid flow and their laminar flows (ESI, Fig. S1). A second T-junction afforded the introduction of Φ_{sheath} using another syringe pump. Exiting this T-junction into a PTFE tubing, the monomer streams were photopolymerized using an UV lamp operating at a wavelength of 365 nm. The polymerized microfibers were collected into a water bath and washed with water and ethanol to remove the residual PEG (Φ_{sheath}) present at the surface of the fibers before air-drying them overnight. The fibers were produced using flow rate of Φ_{core1}, Φ_{core2}, and Φ_{sheath} (Q_{TPGDA}, Q_{NOA89}, and Q_{sheath}) of 2.6, 1.0, and 700 µL/min respectively. The fibers were characterized by numerical and scanning electronic microscopies (Fig. 1b and 1c) exhibiting the two distinct parts composing the Janus fibers and no significant degradation of the fibers after 8 months (ESI, Fig. S2). Furthermore, an arrangement of three side-by-side capillaries was obtained by adding another T-junction and sleeve arrangement to the capillary based microfluidic system shown in Fig. 1a. Hecate microfibers composed of three different materials originating from three monomers, *i.e.* TPGDA, NOA89, and poly(ethylene glycol) diacrylate with a molecular weight of 575 g/mol (PEGDA575), delivered through syringe pumps were prepared in a similar manner with a flow rate equal for all three core phases of

0.7 µL/min and Q_{sheath} = 1200 µL/min. Numerical and scanning electronic microscopies (Fig. 1d and 1e) showed the three phases of the Hecate fiber that were well-merged.

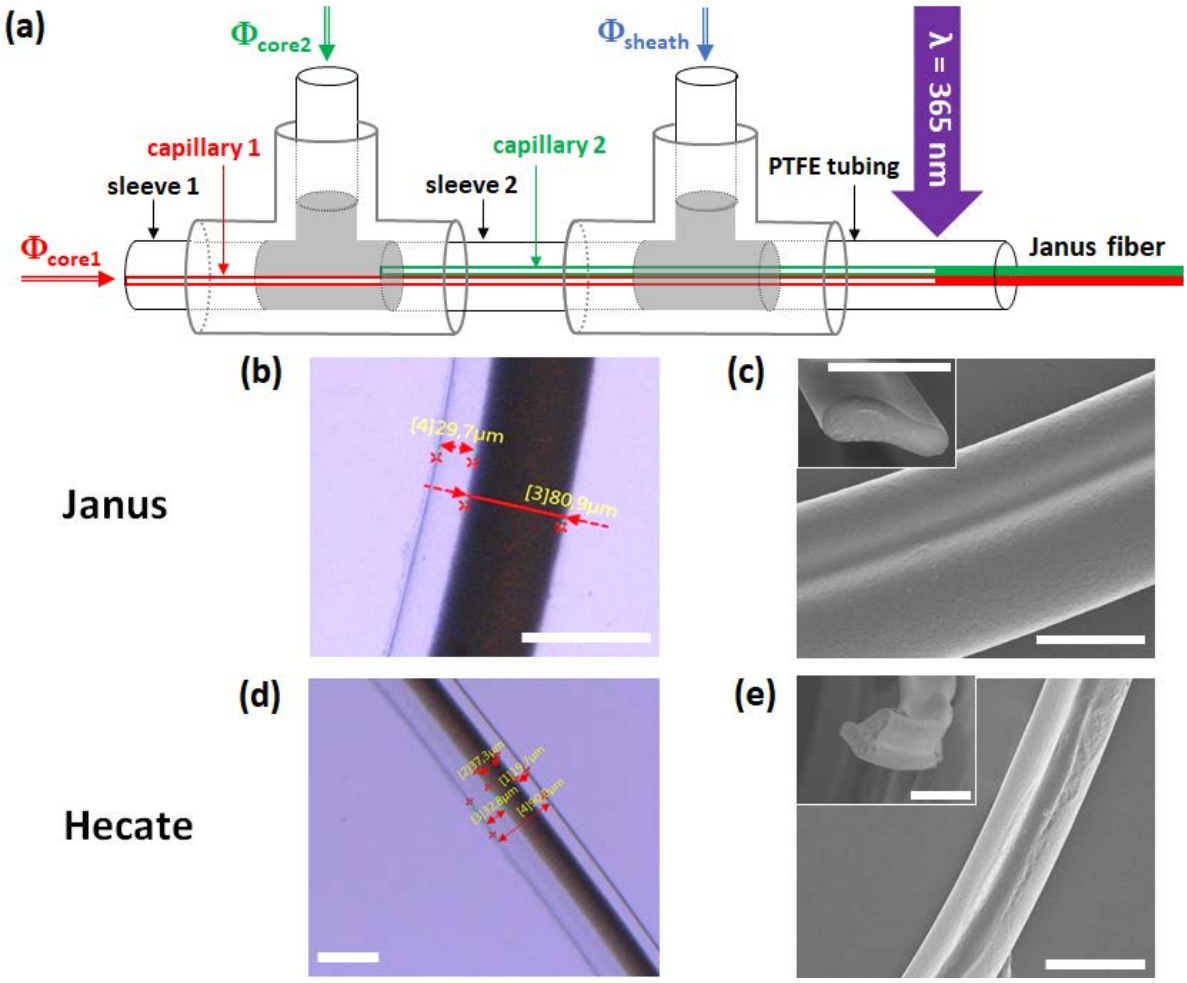

Fig. 1 Janus and Hecate fibers prepared using PEG300 as sheath phase: (a) schematics of the microfluidic side-by-side capillaries system used to produce Janus fibers using TPGDA and NOA89 as core phases and the characterization of Janus (b, c) and Hecate (d, e) fibers by numerical (b and d, poly(TPGDA) observed in dark color) and scanning electron (c and e, fiber cross-section in inset) microscopies. Scale bars = 100 µm.

Morphological characteristics of Janus fibers (*e.g.* diameter) can be tuned by varying the volume contribution of each individual core phase as reported for electrospinning.[6] The flow rate of one of the core phases, either Q_{TPGDA} or Q_{NOA89}, was varied while keeping constant the flow rate of the other core phase. For each experiment the widths of both part of the Janus fiber was measured by numerical microscopy (ESI, Fig. S3) and their variations plotted (Fig. 2a and 2b). The width and therefore the volume of each part of the fiber increased with an increase in the flow rate of the respective monomer as we reported for single fibers.[26] Due to the faster diffusion of

the less viscous core phase into Φ_{sheath}, the corresponding part of the Janus fiber had a larger diameter (*i.e.* TPGDA). However, as expected, the part of Janus microfiber with constant monomer flow rate showed almost the same width. This clearly demonstrated that individual flow rate of core phases can control the volume of each part of the Janus fiber. Dynamic mechanical analysis (DMA) was performed on NOA89/TPGDA Janus microfibers to determine their elastic modulus and compare them to fibers solely composed of NOA89 having a diameter of 162 µm (Fig. 2c). Two Janus microfibers obtained from different ratios of core phase flow (*i.e.* 3.5/1.5 and 3/2.5) affording fibers with different widths (75/45 µm and 63/71 µm) were considered. The presence of TPGDA increased noticeably the elastic modulus of pure NOA fiber (35 MPa) by almost twice for NOA89/TPGDA 75/45 (74 MPa) and up to five-fold for NOA89/TPGDA 63/71 (155 MPa). The results could not be compared to pure TPGDA fibers due to their high fragility rendering the DMA measurement not possible. The mechanical properties of a microfiber could be thus easily tuned according to the needs of the application by producing Janus fibers from two material having different mechanical properties. It is worth noticing that all the images presented in this work for the Janus microfibers as well as mechanical tests revealed no delamination of the microfibers. This probably originated from the interdiffusion of monomers in each other phases during the co-flow of the core phases which upon UV-induced polymerization strongly linked the materials together. This is another advantage of the microfluidic spinning technique which allows starting from miscible monomer phases.

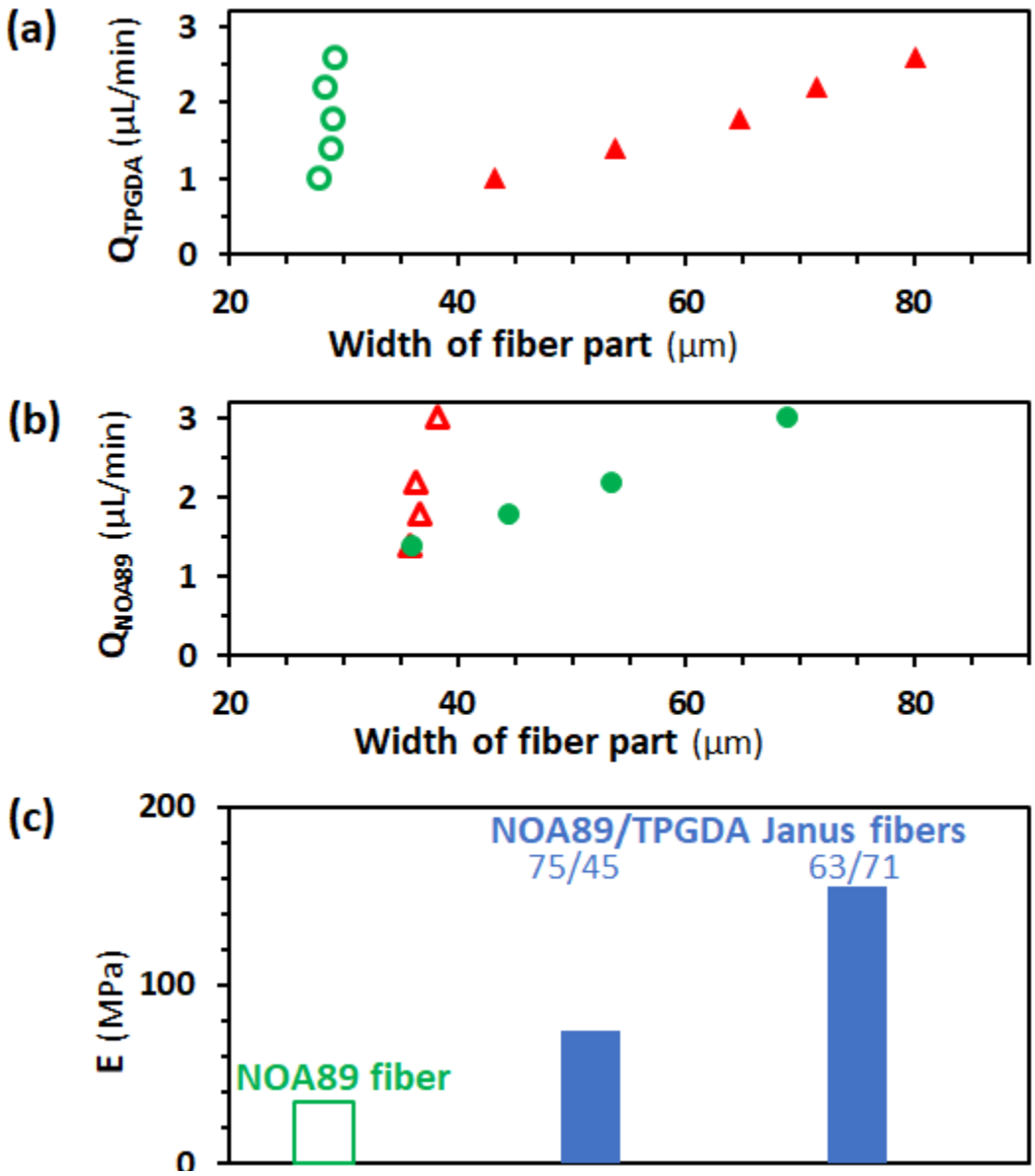

Fig.2 Janus fibers from NOA89/TPGDA: (a) effect of Q_{TPGDA} on the width of poly(TPGDA) part (▲) and cured NOA89 part (○) of Janus fibers for Q_{NOA89} = 1.0 µL/min, (b) effect of Q_{NOA89} on the width of poly(TPGDA) part (△) and cured NOA89 part (●) for Q_{TPGDA} = 0.5 µL/min, and (c) comparison of the elastic modulus (E) of pure crosslinked NOA89 fibers with crosslinked NOA89/poly(TPGDA) Janus fibers by DMA.

To evaluate the robustness of the microfluidic spinning technique, a library of Janus microfibers (Fig. 3) was produced using different acrylic monomers including NOA74 (another photocurable acrylate prepolymer), acrylamide (Am), *N*-isopropyl acrylamide (NIPAm), poly(ethylene glycol) diacrylate with a molecular weight of 400 g/mol (PEGA400), *n*-butyl acrylate (*n*-BA), and *tert*-butyl acrylate (*tert*-BA). In the case of monovinylic monomers, 4 mol% of crosslinker was added (methyl bisacrylamide for Am, PEGDA250 for *n*-BA and *tert*-BA) to ensure the fibers to be stable. All the combinations considered showed a clear interface between the two parts of the Janus

fibers without delamination regardless of their different chemical natures (hydrophilic, hydrophobic, etc.). Amphoteric Janus fibers were thus prepared using an anionic monomer (acrylic acid, AA, 80 v% in water) as Φ_{core1} and a cationic one (2-dimethylamino) ethyl acrylate, DMAEA, 80 v% in water) as Φ_{core2} (Q_{core1} = 1.5 µL/min, Q_{core2} = 3.0 µL/min, Q_{sheath} = 550 µL/min). Irgacure 2959 (4 wt/v%) was used as photoinitiator instead of Irgacure 369 to be soluble in the core phases. These fibers were investigated for their potential to simultaneously remove cationic and anionic dyes from a solution of different dyes. The dye removal efficiency (RE%) and the associated kinetic were conducted by immersing the fibers into a solution of 20 mg/L of either methylene blue (MB, cationic dye) or alizarin red S (AR, anionic dye) at 20 °C. An aliquot of the solution was withdrawn from the fiber solution at predetermined times for analysis by visible spectroscopy (664 nm for MB and 406 nm for AR). RE% was calculated for each dye and each time point (ESI, Fig. S4I) permitting to determine that the equilibrium was reached after 150 and 300 min for AR and MB respectively reaching a maximal RE% of 80 and 99% respectively. The adsorption mechanism was further studied by considering pseudo-first-order and pseudo-second-order adsorption models (ESI, Fig. S5) exhibiting a better fit for the latter one with theoretical and experimental values of the adsorption capacity at the equilibrium (q_e) relatively close for both dyes (ESI, Table S1). These results indicated that the adsorption of MB and AR could be attributed by the electrostatic attractions of oppositely charged active sites on fibers.[28] The adsorption capacity (q_e) for both dyes increased with the increase in the initial concentration in dye (Fig 4a): at lower concentrations the increase was steeper approaching a plateau value at higher concentrations. Higher adsorption capacity at high concentration is due to the presence of large concentration gradient of dye molecules and adsorbents sites which results in the increase in mass transfer between adsorbent and dye molecules due to larger electrostatic attractions.[29] To evaluate the maximum adsorption capacity of the amphoteric Janus fibers, surface properties and interaction of dye molecules with Janus fiber, the Langmuir and Freundlich isotherm models were applied on the data represented in Fig. 4a (ESI, Fig. S7, Table S1). The data better fitted to the Langmuir isotherm for both dyes showing that the adsorption followed a monolayer homogenous mechanism and the separation constant (R_L) was comprised between 0 and 1 for both dyes (ESI, Table S2) showing the higher affinity and favorability of adsorption of dyes with the adsorbent.[30] Furthermore, the favorability of adsorption of MB and AR was confirmed through the Freundlich isotherm model, where the value of n for both dyes was found in the region ($0 < n < 10$). Another parameter of interest is the pH of the solution that was varied between 3 and 11 (Fig. 4b and ESI, Fig. S5). The adsorption of MB increased from pH 4 to 7 reaching 100% of RE% and maintaining a plateau for higher values of pH. The decrease in adsorption at acidic pH was attributed to the protonation of the carboxylic acid groups reducing the charges accessible for adsorption of the dye at the surface of the poly(AA) part of the Janus fibers. Conversely, the adsorption of AR decreased with increased pH values that could be associated to the deprotonation of the amines and thus lowering the number of sites for AR to adsorb. The adsorption capacity of these fibers for either MB or AR are comparable or superior to materials reported in the literature (ESI, Table S3) considering that most reports are on

nanofibers which could have a strong influence on the adsorption capacity due to the higher surface to volume ratio. The adsorption capacity of these amphoteric Janus fibers was compared with fibers having a single part produced with both AA and DMAEA using the same feed composition in monomers and flow rate conditions as for the Janus fibers (Fig. 4c). For each dye and concentration considered, the adsorption capacity of the amphoteric Janus fibers was observed to be superior. This could be due to the lower propensity of the comonomers to neutralize their charges in this structure due to the reduced area in which the monomers of opposite charges were in close proximity to the interface between the two parts of the Janus fibers. The simultaneous removal of both dyes by the amphoteric Janus fibers at pH 6.5 showed a slight decrease in adsorption capacity as compared to when only one dye was used (Fig. 4c) which could be due to (i) the specific pH requirement of each dye (pH = 7 for MB, pH = 6 for AR) and (ii) saturation and/or complexation of dyes in the solution leading to their precipitation (ESI, Fig S8). Recycling capability is one of the crucial factors in evaluating the adsorbent performance. Cationic and anionic dyes could be desorbed using acidic and basic solutions. The fibers adsorbed with MB and AR were soaked into a 0.1 mol/L solution of hydrochloric acid and potassium hydroxide. Four cycles of adsorption-desorption were performed showing a very slight decrease in adsorption efficiency without affecting the appearance of the fibers (ESI, Fig. S9). The decrease may be due to incomplete desorption of adsorbate and loss of active sites during regeneration associated to the protonation and deprotonation of the carboxylic acid and amine groups.[28]

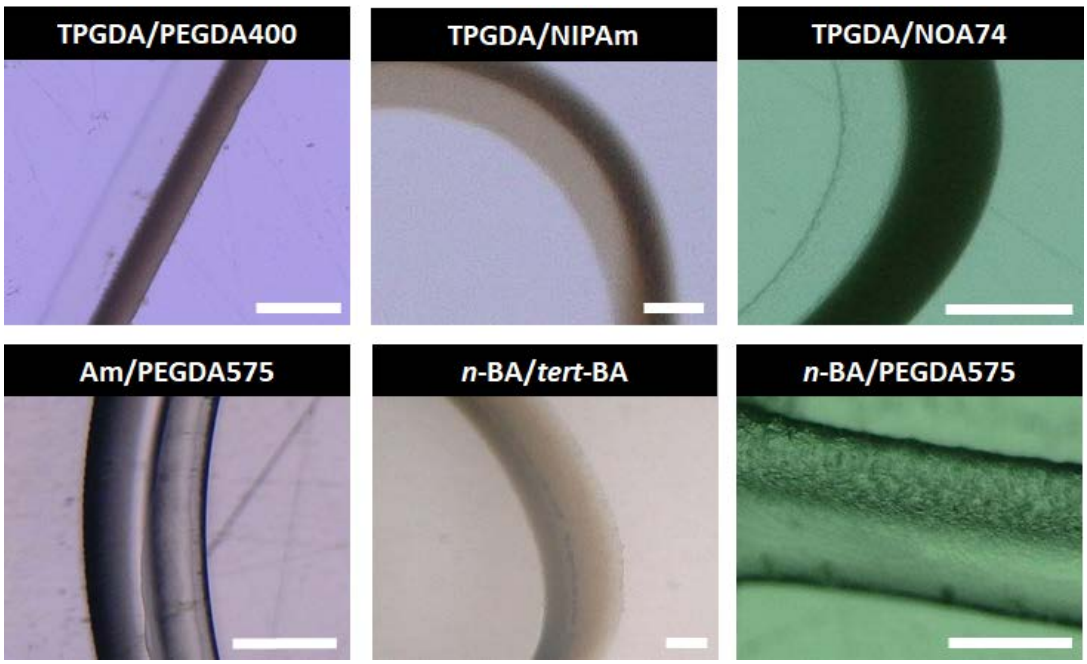

Fig. 3 Numerical microcopy images of Janus fibers produced using different monomer combinations (scale bar = 100 µm). The differences in background colors is due to the contrast corrections done to better observe both parts of the Janus microfibers.

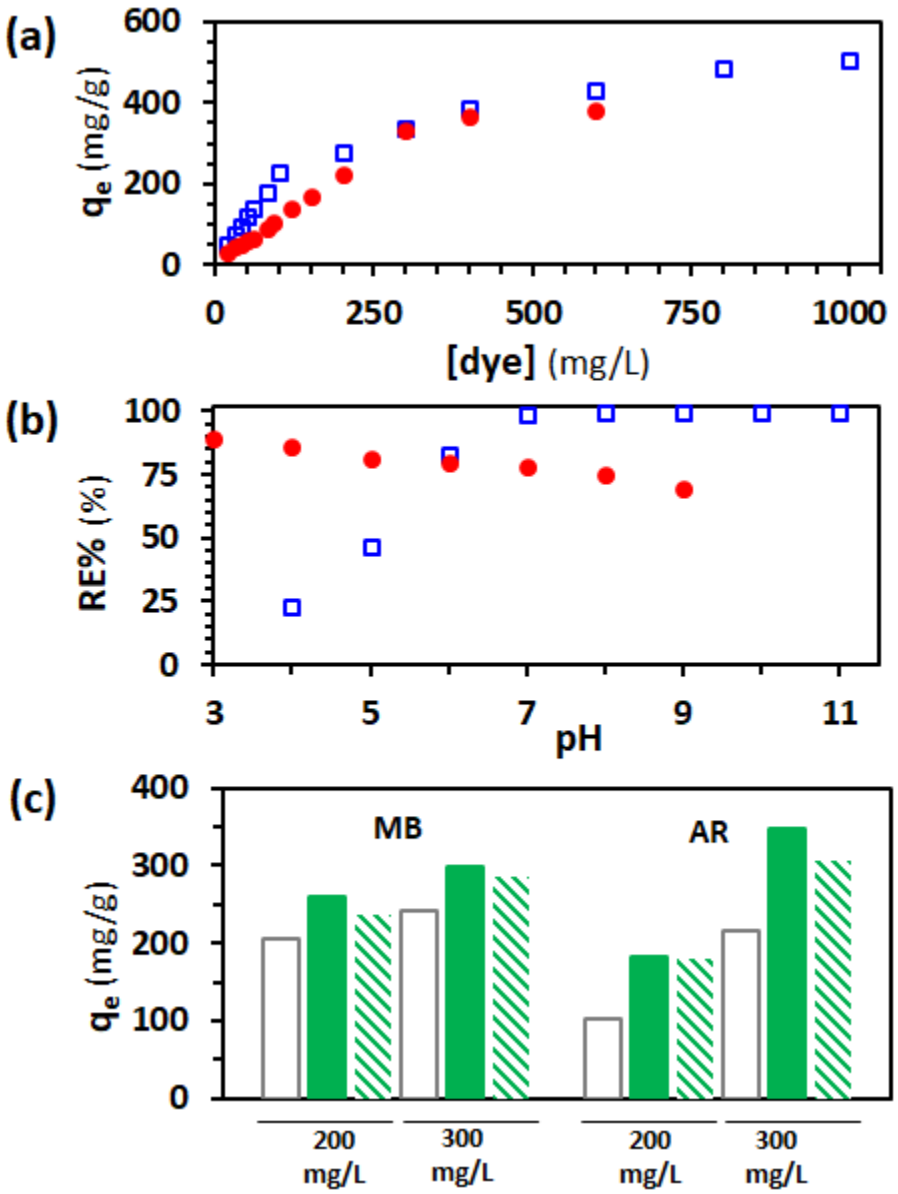

Fig.4 Amphoteric AA/DMAEA Janus fibers and their capacity to adsorb dyes (MB = methylene blue = □, AR = alizarin red S = ●): effect of the (a) initial dye concentration on the adsorption capacity (q_e) and (b) pH on the dye removal efficiency (RE%), and (c) comparison of fibers with a single part of a copolymer of AA and DMAEA (empty bars, grey border) with Janus fibers (green bars) when exposed to a single dye (filled) and both dyes (diagonal stripes) at 200 and 300 mg/L of dye.

In summary, Janus and Hecate microfibers were successfully produced using a simple microfluidic spinning technique. Miscible core and sheath phases were considered to avoid the formation of droplets associated to the interfacial forces among immiscible phases. The width, and thus the volume, of each individual part of Janus microfibers can be easily tuned by altering the flow rate of one of the monomer phases. Janus microfibers of various chemical natures were successfully prepared offering systems with increased mechanical properties and adjustable properties.

Furthermore, the use of Janus fibers conversely to fibers constituted of a single part with the comonomer composition showed superior performances as illustrated for the removal dye. These results pave the way to the development of multiphase microfibers for a wide range of applications, illustrated here with amphoteric Janus fibers that could be used for the simultaneous removal positively and negatively charges species for water depollution.

WR acknowledges the Higher Education Commission Pakistan for his PhD scholarship. This work of the Interdisciplinary Institute HiFunMat, as part of the ITI 2021-2028 program of the University of Strasbourg, CNRS and Inserm, was supported by IdEx Unistra (ANR-10-IDEX-0002) and SFRI (STRAT'US project, ANR-20-SFRI-0012) under the framework of the French Investments for the Future Program. The authors thank the electron microscopy facilities at the Institut Charles Sadron and Damien Favier for his help with DMA.

Conflicts of interest

There are no conflicts to declare.

Notes and references

1. J. Cheng, Y. Jun, J. Qin and S. H. Lee, *Biomaterials*, 2017, **114**, 121-143.
2. J. Lou, Y. Wang and L. Tong, *Sensors*, 2014, **14**, 5823-5844.
3. X. Y. Du, Q. Li, G. Wu and S. Chen, *Adv. Mater.*, 2019, **31**, e1903733.
4. M. Akella, S. Shabaniverki and J. J. Juárez, *RSC Adv.*, 2020, **10**, 434-443.
5. Q. Huang, F. He, J. Yu, J. Zhang, X. Du, Q. Li, G. Wang, Z. Yu and S. Chen, *J. Mater. Chem. B*, 2021, **9**, 2727-2735.
6. G. Chen, Y. Xu, D. G. Yu, D. F. Zhang, N. P. Chatterton and K. N. White, *Chem. Commun.*, 2015, **51**, 4623-4626.
7. D. G. Yu, C. Yang, M. Jin, G. R. Williams, H. Zou, X. Wang and S. W. Bligh, *Colloids Surf. B Biointerfaces*, 2016, **138**, 110-116.
8. J. Knapczyk-Korczak, J. Zhu, D. P. Ura, P. K. Szewczyk, A. Gruszczyński, L. Benker, S. Agarwal and U. Stachewicz, *ACS Sustainable Chem. Eng.*, 2020, **9**, 180-188.
9. M. Wang, D. Li, J. Li, S. Li, Z. Chen, D.-G. Yu, Z. Liu and J. Z. Guo, *Mater. Des.*, 2020, **196**, 109075.
10. J. Yang, K. Wang, D. G. Yu, Y. Yang, S. W. A. Bligh and G. R. Williams, *Mater. Sci. Eng. C*, 2020, **111**, 110805.
11. X. Cao, J. Deng and K. Pan, *Adv. Fiber Mater.*, 2020, **2**, 85-92.
12. J. Tian, Q. Ma, W. Yu, D. Li, X. Dong, G. Liu and J. Wang, *Mater. Des.*, 2019, **170**, 107701.
13. Y. Srivastava, M. Marquez and T. Thorsen, *Biomicrofluidics*, 2009, **3**, 12801.
14. Z.-C. Yao, J.-C. Wang, B. Wang, Z. Ahmad, J.-S. Li and M.-W. Chang, *J. Drug Deliv. Sci. Technol.*, 2019, **50**, 372-379.
15. L. Ionov, G. Stoychev, D. Jehnichen and J. U. Sommer, *ACS Appl. Mater. Interfaces*, 2017, **9**, 4873-4881.

16. A. L. Thangawng, J. P. B. Howell, C. M. Spillmann, J. Naciri and F. S. Ligler, *Lab Chip*, 2011, **11**, 1157-1160.
17. R. Utoh, S. Enomoto, M. Yamada, K. Yamanaka, Y. Yajima, K. Furusawa and M. Seki, *Mater. Sci. Eng. C*, 2021, **129**, 112417.
18. S.-K. Chae, E. Kang, A. Khademhosseini and S.-H. Lee, *Adv. Mater.*, 2013, **25**, 3071-3078.
19. Y. Cheng, Y. Yu, F. Fu, J. Wang, L. Shang, Z. Gu and Y. Zhao, *ACS Appl. Mater. Interfaces*, 2016, **8**, 1080-1086.
20. J. K. Nunes, H. Constantin and H. A. Stone, *Soft Matter*, 2013, **9**, 4227-4235.
21. W. Lan, Y. Du, X. Guo, A. Liu, S. Jing and S. Li, *Ind. Eng. Chem. Res.*, 2017, **57**, 212-219.
22. A. Perazzo, J. K. Nunes, S. Guido and H. A. Stone, *Proc. Natl. Acad. Sci. U. S. A.*, 2017, **114**, E8557-E8564.
23. W. Jeong, J. Kim, S. Kim, S. Lee, G. Mensing and D. J. Beebe, *Lab Chip*, 2004, **4**, 576-580.
24. S. Cho, T. S. Shim and S.-M. Yang, *Lab Chip*, 2012, **12**, 3676-3679.
25. M. A. Daniele, K. Radom, F. S. Ligler and A. A. Adams, *RSC Adv.*, 2014, **4**, 23440-23446.
26. W. Razzaq, C. A. Serra, L. Jacomine and D. Chan-Seng, *J. Taiwan Inst. Chem. Eng.*, 2022, **132**, 104215.
27. C.-H. Choi, H. Yi, S. Hwang, D. A. Weitz and C.-S. Lee, *Lab Chip*, 2011, **11**, 1477-1483.
28. A. Shen, X. Liao and Y. Li, *Colloids Surf. A*, 2021, **623**, 126666.
29. R. B. Gapusan and M. D. L. Balela, *Mater. Chem. Phys.*, 2020, **243**, 122682.
30. C. Lei, F. Wen, J. Chen, W. Chen, Y. Huang and B. Wang, *Polymer*, 2021, **213**, 123316.